

Pilot-scale evaluation of forward osmosis membranes for volume reduction of industrial wastewater

Joel Minier-Matar, Mashael Al-Maas, Altaf Hussain, Mustafa S. Nasser, Samer Adham

Item type

Journal Contribution

Terms of use

This work is licensed under a [CC BY 4.0](https://creativecommons.org/licenses/by/4.0/) license

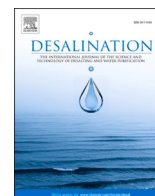
This version is available at

https://manara.qnl.qa/articles/journal_contribution/Pilot-scale_evaluation_of_forward_osmosis_membranes_for_volume_reduction_of_industrial_wastewater/26095432/1

Access the item on Manara for more information about usage details and recommended citation.

Posted on Manara – Qatar Research Repository on

2022-06-01



Pilot-scale evaluation of forward osmosis membranes for volume reduction of industrial wastewater

Joel Minier-Matar^a, Mashael Al-Maas^a, Altaf Hussain^a, Mustafa S. Nasser^b, Samer Adham^{a,c,*}

^a ConocoPhillips Global Water Sustainability Centre, Qatar Science & Technology Park, Doha, Qatar

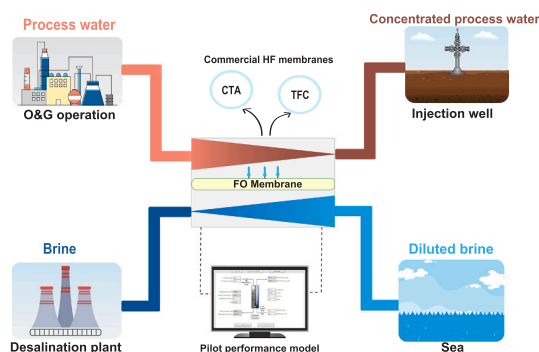
^b Gas Processing Centre, College of Engineering, Qatar University, Doha, Qatar

^c Center for Advanced Materials, Qatar University, Doha, Qatar

HIGHLIGHTS

- Side-by-side pilot study of 2 commercial FO membranes with industrial wastewater
- TFC showed higher water flux (9.9 vs 1.7 L/m²·h) compared to cellulose triacetate.
- CTA showed 13% fouling due to calcium phosphate scaling; TFC showed <5% fouling
- Certain hydrophilic organics can pass through CTA but not TFC module.
- Citric acid cleaning restored the CTA module flux back to their initial performance.

GRAPHICAL ABSTRACT



ARTICLE INFO

Keywords:

Osmotic concentration
Wastewater treatment
Oil and gas
Full-scale
Commercial modules
Natural osmosis

ABSTRACT

Water treatment is a key aspect for the sustainable management of oil & gas operations. Osmotic concentration (OC) is an advanced water treatment process, adapted from forward osmosis (FO), that does not require water recovery from the draw solution. In this study, two commercial hollow fiber FO membranes [Module 1, cellulose triacetate (CTA) and Module 2, thin film composite (TFC)] were evaluated at pilot scale using actual process water obtained from a gas production facility. The evaluation focused on assessing the membrane productivity, fouling potential and chemical cleaning efficiency while normalizing the performance using a theoretical model that account for the variability of the operating conditions. Performance tests showed that Module 2 has a higher flux compared to Module 1, 9.9 L/m²·h vs 1.7 L/m²·h; and lower specific reverse solute flux (RSF) for most of the ions. Additionally, Module 1 benchmark experiment showed a 13% flux loss attributed to inorganic fouling (calcium phosphate precipitation) while the flux loss in Module 2 was <5% possibly due to enhanced module hydrodynamics and variation in membrane chemistry. Chemical cleaning (citric acid) proved to be successful in restoring the flux for Module 1. From the 8.1 mg/L organic carbon present in the feed, advanced organic characterization revealed that certain group of hydrophilic organics are able to pass through Module 1, but not Module 2, translating to a specific forward organic solute flux of 0.9 mg/L and 0.1 mg/L for Module 1 and 2, respectively. Finally, key sustainable and environmental considerations were presented in support of further development of process implementation. The OC process has strong potential for full-scale installation; however,

* Corresponding author at: Center for Advanced Materials, Qatar University, Doha, Qatar.

E-mail address: sadham@qu.edu.qa (S. Adham).

<https://doi.org/10.1016/j.desal.2022.115689>

Received 29 December 2021; Received in revised form 18 February 2022; Accepted 5 March 2022

Available online 21 March 2022

0011-9164/© 2022 The Authors. Published by Elsevier B.V. This is an open access article under the CC BY license (<http://creativecommons.org/licenses/by/4.0/>).

demonstrating its performance in the field would be the next step necessary for successful implementation of the technology.

1. Introduction

During oil & gas extraction and production, large volumes of water are brought to the surface (called produced water) or generated during oil & gas processing (called process water) [1]. In conventional operations, 3 to 4 barrels (500 to 600 L) of water are generated for every barrel (160 L) of oil extracted from the ground [1]. As the reservoir age, this ratio could increase up to 10 barrels of water (1600 L); thus, efficient water management is key for the sustainable development of oil & gas fields [2–5]. Large amount of produced and process water are also generated from gas fields [3,6].

Even though several water streams can be cost-effectively treated for either reuse or surface discharge, the majority of the water is currently injected into deep disposal wells [7] since that option typically requires limited treatment, including removal of hydrogen sulfide and suspended solids, and pH neutralization; but those requirements depend on the environmental regulations of each country [8]. Typically, disposal wells have limited capacity, and drilling additional wells is very costly [9]; especially if they are located offshore. Reducing the volume of water sent to deep well injection, would increase the service life of the wells and minimize the need for drilling new disposal wells.

Gas field wastewaters are typically characterized by their lower salinity (<5000 mg/L) compared to conventional oil wells [2,3]; which presents an attractive opportunity for recycle and/or reuse. In Qatar, process water generated from natural gas production, is treated using membrane bioreactor (MBR) and reverse osmosis (RO) reducing wastewater disposal/injection volumes while generating permeate to be reused as boiler feed water [10]. In Australia, the coal seam gas produced water is treated using ultrafiltration followed by RO and the permeate is used for beneficial reuse in agricultural applications [11]. However, advanced treatment schemes come at a significant water management cost [12–18].

Osmotic concentration (OC) is an advanced water treatment process that has been adapted from forward osmosis (FO). In OC, the feed and draw solutions flowed in different sides of a semi-permeable membrane, where water from the feed solution flows through the membrane into the draw solution, proportionally to the concentration gradient across the membrane. Since OC does not require recovery of the draw solution, it is mainly a volume reduction process (for feed solution) or dilution process (for draw solution); thus, OC could be applied to cost-efficiently reduce the volumes of low salinity produced and process water if a relatively high salinity water stream is available nearby [19–22].

The OC process operates under lower pressure (typically atmospheric) minimizing the amount of energy required when compared to the state-of-the-art RO process. Since it is not a physical pressure driven process, OC has less fouling tendency in comparison to RO [23–25]. The drawback is that the process doesn't produce permeate water for reuse.

Previously our team evaluated OC process to reduce the gas field produced and process water volumes via bench scale testing [26,27]. Results were promising showing stable FO membrane flux and excellent organic rejection. Also, superior performance was observed for hollow fiber (HF) configuration when compared to flat sheet, offering the following advantages [26,28]:

- Higher packing density, reducing footprint (the physical area occupied by the membranes) [29–31].
- Improved hydrodynamics minimizing fouling propensities [23].
- Self-supported, eliminating the need for spacers and potentially reducing fouling [32].

Although, the impact of module configuration on FO membrane

fouling has not been widely study, researchers have reported comparisons between flat sheet and HF fouling rates in different applications. Howe et al. conducted side-by-side microfiltration and ultrafiltration experiments which proved that flat sheet membranes typically foul more rapidly than HF membranes under similar conditions [33]. Dardor et al. evaluated the performance of flat sheet vs HF membranes for pressure retarded osmosis and concluded that FO HF is less susceptible to fouling [34]. Those studies provide some indication that HF membranes could also be less prone to fouling; however detailed experimental evaluations remain necessary to validate this claim.

Currently, limited pilot studies are available in the literature for treatment of real wastewaters by FO [35,36]. Oasys evaluated OC technology based on thermally recoverable ammonium carbonate draw solution and carried pilot investigation for treatment of high salinity produced water in US [37]. The technology was also applied for zero liquid discharge for the treatment of coal fired power plant wastewater in China [38]. FO-RO has been applied for the treatment of raw produced water; the system achieved more than 99% rejection of almost all the ions, but fouling was observed due to the organic constituent present in the produced water. The team concluded that membrane cleaning and pretreatment are needed for stable operation of the process [39]. Hydration Technology Innovations (HTI) implemented FO process for produced water volume minimization and reclaimed the water for reuse in hydraulic fracturing [29]. Another pilot evaluation of the osmotic dilution process consisted of applying FO/RO to integrate seawater desalination with municipal wastewater treatment using a plate and frame membrane module from Porifera. The study focused on understanding and developing fouling index for FO process that can be used in assessing process performance and determining fouling and cleaning frequencies [40]. Studies have also shown that advanced pretreatment is key to ensure FO membrane integrity. Researchers have evaluated pressure assisted FO (PAFO) in a pilot unit for seawater desalination using spiral wound FO element from Toray concluding that advanced pretreatment process for bacterial removal and organic matter is needed for FO membrane integrity [41]. Researchers have also focused on evaluating different membrane chemistries, cellulose triacetate (CTA) and thin film composite (TFC) have been extensively studied and used in the development of forward osmosis membranes [42–45].

As seen above, there has been some FO pilot studies that aimed to increase the technology readiness level (TRL) of the process. However, most of the evaluations focus on testing one type of membrane and have not performed side by side comparison for different FO membrane modules, under similar conditions. This type of comparison is critical in determining which product material or configuration is more suitable for the treatment of produced or process water within the oil & gas industry. Additionally, very limited pilot studies are available on evaluating HF membrane configuration at pilot scale using actual wastewater from industrial facilities [35,36].

In order to scale up the OC process, our team previously screened various full-scale HF membrane modules in a bench-scale batch operation and identified commercial FO modules suitable for pilot evaluation [46,47].

The present investigation compares two commercial HF - FO membranes side by side, at pilot scale, using actual industrial wastewater to compare membrane productivity, fouling propensities, and cleaning efficiencies and also identify key factors that are critical for full-scale implementation of the technology. The specific objectives of this paper are to:

- Assess the performance (flux and fouling) of two commercial FO membranes at pilot scale level using actual process water from a natural gas processing facility,
- Apply advanced methodologies to evaluate membrane characteristics and water quality, and
- Identify sustainable and environmental considerations for full-scale implementation of OC.

2. Materials & methods

2.1. Feed & draw solution water quality

Membranes were tested using actual wastewater (WW) which was a mixture of different streams generated from a natural gas processing facility in Qatar. Prior to collection, pretreatment of the actual WW included a full-scale MBR for suspended solids and dissolved organics removal [48]. A total volume of 5 m³ of the pretreated WW was collected from the processing facility and transferred to the pilot site where the pilot evaluation was conducted.

Synthetic seawater was used as the draw solution (DS) to eliminate potential interferences by organics present in actual seawater and thus focus the membrane performance evaluation on the actual WW. Targeting the salinity of the Arabian Gulf seawater (i.e., ~40,000 mg/L), the DS was prepared using NaCl and dechlorinated tap water. Since osmotic concentration does not require draw solution recovery, the diluted draw solution (diluted seawater) can be disposed directly to the sea.

Benchmark tests, using synthetic feed solution (FS), were used to evaluate membrane integrity and stability prior to actual wastewater (WW) testing. Benchmark tests were also performed after the actual WW and chemical cleaning tests to assess membrane fouling, and cleaning efficiency. The synthetic FS (2000 mg/L NaCl) was prepared using tap water pretreated with activated carbon for chlorine removal [46,49].

Table 1 illustrates the water quality data for synthetic feed, real wastewater and synthetic draw solution used in pilot testing. The scaling potential of the industrial wastewater was calculated using OLI Stream Analyzer 9.0 (OLI Systems Inc., Morris Plains, NJ, US). Additionally, the membrane reverse solute flux (RSF) was calculated based on the ionic composition of the feed solution at the beginning and end of the test to determine the organic and inorganic passage through the membranes.

2.2. Pilot unit

A custom-built pilot testing unit was designed and assembled to allow testing of different hollow-fiber FO membrane modules (Figs. 1 and 2). The unit can operate in one-pass configuration (without

recycling the feed or draw solution) and in feed and bleed mode (partial recirculation), which allows the recycle of either feed or draw solution, or both. The unit consisted in two identical loops, one for the feed and the other for the draw solution. Each loop is equipped with sensors for monitoring temperature, pressure, and conductivity. Positive displacement pumps (KNF, Switzerland) were used to circulate the water within the loops. Cartridge filters (5 µm, Atlas Filtri, Italy) were installed ahead of the membrane module for removal of suspended solids. A LabVIEW real-time system (cRIO 9035, NI, USA) was employed to control the unit operation, to record the performance parameters and to maintain constant flow rates based on a proportional–integral–derivative (PID) controller [50].

For “one-pass” operating mode (Module 1 – Fig. 1A), the water flux was calculated using flowmeters installed at the inlet and outlet of each stream (Omega, USA). For feed and bleed operation (Module 2 – Fig. 1B), the flux was calculated based on the difference in weight of an intermediate buffer tank (20 L) using a balance (Mettler Toledo, Switzerland) with a capacity of 60 kg connected to the LabVIEW control system. The intermediate tank allowed the feed solution to be concentrated to the target 75% recovery. Once the target value has been reached the control system maintains the concentration constant (±5%) by adding fresh feed based on intermediate tank conductivity readings. When the volume reaches the maximum capacity of the feed tank (20 L), 12 L are transferred from the intermediate tank to the 5 m³ feed concentrate tank.

2.3. Membranes

Two commercially available HF-FO modules were evaluated for the treatment of industrial wastewater. The membranes were selected through a detailed bench scale comparison of various commercial modules based on water productivity, salt and organic rejection, and fouling propensity [46]. The two modules selected were those available as commercial products for pilot testing and they represent different chemistries and manufacturers: cellulose triacetate (CTA, Module 1) and polyamide thin film composite (TFC, Module 2). Details of the modules are presented in Table 2.

Module 1 has an active membrane area of 31.5 m² and operates in one-pass mode, without recirculation of the feed or draw solution. The draw solution flowed in the lumen side of the fibers while the feed solution flowed in the shell.

For Module 2, with an active membrane area of 0.5 m², the feed solution was recirculated but not the draw solution. For this module, the feed solution was flowing in the lumen side while the draw solution flowed in the shell.

2.3.1. Microscopic analysis

Microscope analysis of the fibers highlights the difference between the fiber sizes for both membranes. As seen in Fig. 3A, Module 1 fibers are hair-like looking with a diameter of approximately 130 µm, within the range reported by others [51]. On the other hand, Module 2 had a diameter of 1080 µm [30], 10× larger than Module 1. Fig. 3B and C showed the cross sections of the fiber from Module 1 and 2 respectively, highlighting their different inner diameters.

2.4. Mode of operation

Since the modules have different chemistries, membrane areas, and fiber sizes, the operating conditions for each module were determined based on the manufacturers' design and specifications to ensure optimum membrane performance on achieving the target 75% recovery. Those conditions include feed and draw flowrates and location (inside or outside the lumen), mode of operation (one-pass or feed and bleed recirculation) and the cleaning protocol.

Module 1 was evaluated in one-pass operation without recirculating the feed or draw solutions (Fig. 1A). In this operating mode, the module

Table 1
Water quality data for feed and draw solutions.

Parameter	Unit	FS	FS	DS
		Synthetic	Actual WW	Synthetic
pH		7.9	7.1	7.7
Conductivity	µS/cm	4000	2154	64,000
Turbidity	NTU	0.2	0.3	0.7
Total dissolved solids	mg/L	2424	946	41,051
Total suspended solids	mg/L	<5	<5	<5
Inorganic carbon	mg/L	19	76	15
Total organic carbon	mg/L	0.3	8.1	0.7
Chloride	mg/L	1453	253	24,551
Sodium	mg/L	971	422	16,500
Sulfate	mg/L	<0.1	245	<5
Phosphate	mg/L	<0.1	18	<5
Calcium	mg/L	<0.1	3.3	<5
Magnesium	mg/L	<0.1	3.2	<5
Iron	mg/L	<0.1	<0.1	<5
Strontium	mg/L	<0.1	<0.1	<5
Residual Cl ₂	mg/L	<0.1	<0.1	<0.1

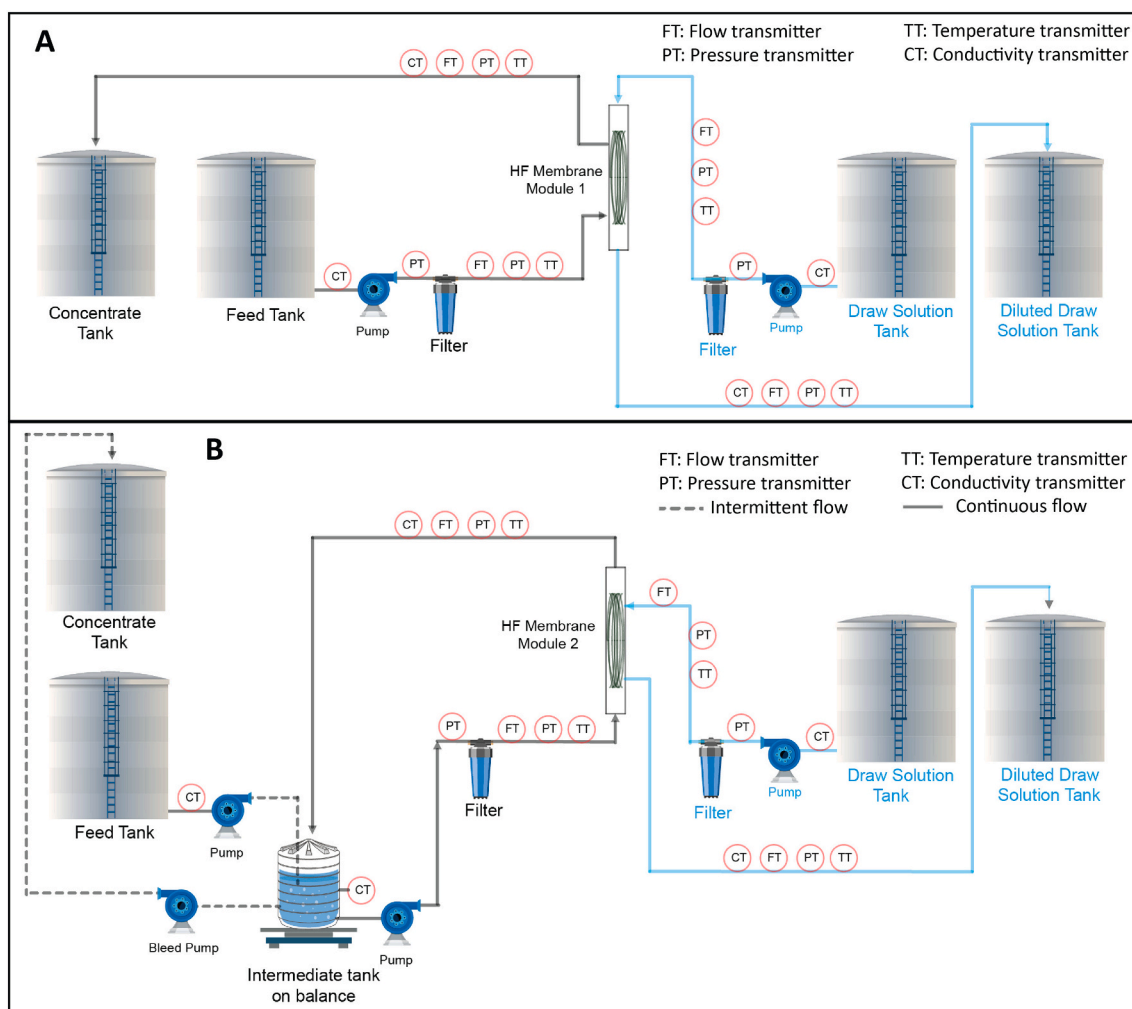


Fig. 1. Custom built pilot unit. A) Operating mode for Module 1: One-pass. B) Operating mode for Module 2: Feed and Bleed.

can achieve the desired recovery due to its large membrane area. Based on manufacturer's specifications, Module 1 operated in counter-current mode with the draw solution flowing in the fiber lumen and the feed solution flowing in the shell.

Module 2 has a lower membrane area compared to Module 1 (Table 2) and it was also tested in counter-current mode. To achieve the 75% recovery, Module 2 operated in feed and bleed mode (Fig. 1B). Based on manufacturer's specifications, the draw solution flowed inside the shell in one-pass operation while the feed solution flowed in the lumen in feed and bleed recirculation. At the start of the experiment, feed solution was concentrated from its initial salinity until reaching 75% recovery (concentration phase); then the module operated in feed and bleed mode where fresh feed water was added periodically into the intermediate feed tank (approximately 1-2 L based on the intermediate tank conductivity readings) to maintain the concentration at the 75% recovery $\pm 5\%$. Once the intermediate tank reached its maximum capacity (20 L), 12 L were automatically transferred to the feed concentrate tank.

2.5. Membrane cleaning

The cleaning procedures for each module were selected based on manufacturers' recommendations to ensure compatibility with the different membrane chemistries.

For inorganic removal, a 2% citric acid solution (pH between 3 and 4) was recirculated through the feed channel of each module for 15 min.

After each cleaning cycle, the membranes were flushed with dechlorinated tap water.

For organic fouling removal, a 10 mmol/L sodium dodecyl sulfate (SDS) solution, adjusted to pH 4 using HCl, was used to clean Module 1. The cleaning solution was recirculated through the shell of the module for 15 min [52]. For Module 2, a 6 mmol/L NaOH solution (pH 11) was recirculated within the fiber lumen for 15 min.

The efficiency of chemical cleaning was evaluated by comparing the water flux (before and after cleaning) with the theoretical predicted value from the model (Section 3); less deviation from the model prediction, translates to more effective cleaning.

2.6. Chemical analysis

Table 3 lists the laboratory analyses applied for characterizing the composition of the feed and draw solutions as well as to ensure that residual chlorine concentration in test solutions was below 0.1 mg/L, the specified membrane tolerance range for Module 2. The table also lists the advanced techniques applied to characterize the fouling mechanism of the membranes.

2.6.1. Inorganic analysis

Anions and cations analysis were performed using ion chromatography (ICS 6000, Thermofisher, USA). Electrically generated eluents, KOH and MSA, were used to inject the samples into the anion and cation separation columns (AS19 and CS12A) follow by conductivity

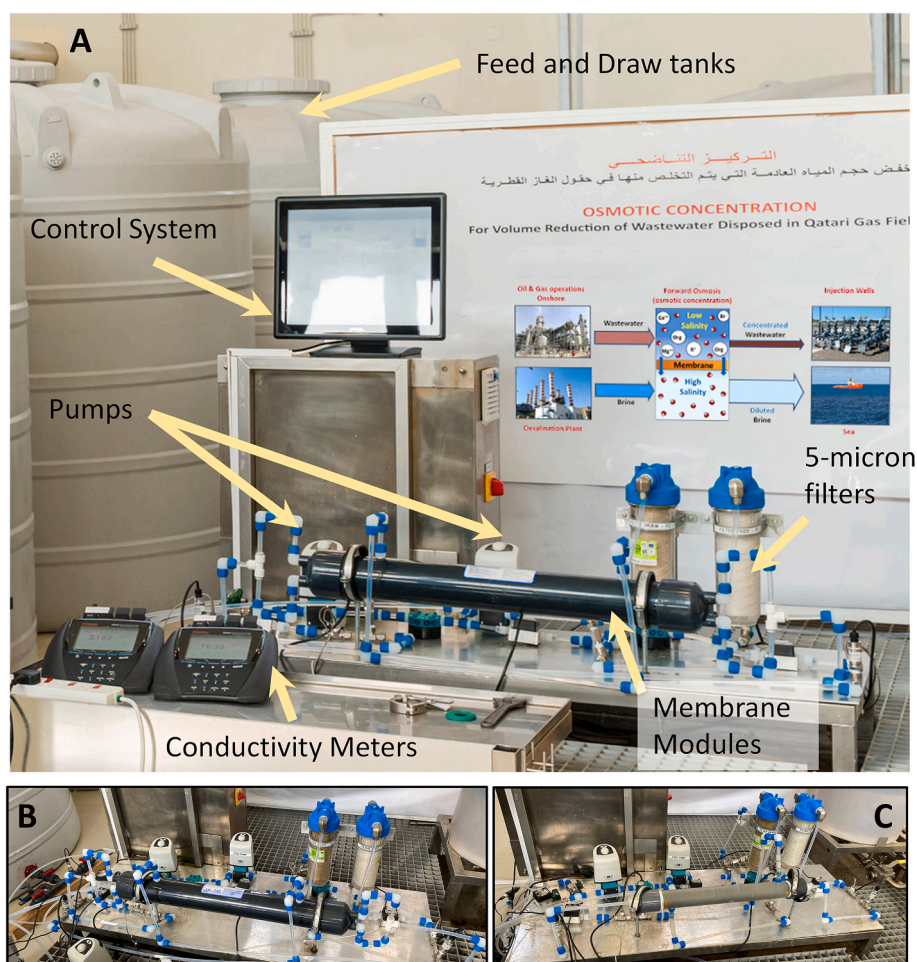


Fig. 2. Custom built pilot unit. A) Overall unit with primary components. B) Module 1, C) Module 2.

Table 2
Membrane properties.

Parameter	Units	Module 1	Module 2
		Toyobo HPC3205	Aromatec 2"
Material		Cellulose triacetate (CTA)	Thin film composite (TFC)
Membrane area	m ²	31.5	0.5
Configuration		Hollow fiber	Hollow fiber
Feed solution		One-Pass	Feed and bleed
Draw solution		One-Pass	One-Pass
Operating mode			
K _m - mass transfer coefficient	L/(m ² ·h)	0.0150	0.0069
A - Water permeability	20 °C	0.195	2.268
	25 °C	0.228	2.805
	30 °C	0.260	3.343
B - Solute permeability	20 °C	0.050	0.319
	25 °C	0.054	0.391
	30 °C	0.059	0.464
Fiber inner diameter	μm	70	780
Fiber outer diameter	μm	130	1080
Membrane thickness	μm	30	150
Shell diameter	mm	90	60
Module active length	mm	560	430

measurements to determine the ion concentration. The system was calibrated using commercial standards from ThermoFisher Scientific, USA.

Metals were measured using inductively coupled plasma (ICP); samples were acidified with nitric acid (2%) prior analysis. Samples were injected into the ICP and iron and strontium measured in radial mode at wavelengths of 238.204 nm and 407.771 nm respectively.

2.6.2. Organic analysis

Organic compounds in the various water streams were characterized based on their hydrophobicity and hydrophilicity as well as on their molecular weight. This advanced organic characterization is unique in identifying hydrophobic compounds that may foul the membranes.

For this analysis, a custom-built chromatography system was assembled (Fig. 4); the system consisted of a high-pressure liquid chromatography (LC) pump (ICS 5000+, ThermoFisher Scientific, USA), a size exclusion chromatography column and a total organic carbon (TOC) detector (M9-SEC, Sievers, USA). The size exclusion chromatography column was packed with Toyopearl HW50S resin (Repel, Germany), which is a super hydrophilic resin with particle size between 20 and 40 μm. The M9-SEC TOC detector is capable of continuous analysis of total organic carbon with a response time of 4 s. The detector measured the TOC based on persulfate oxidation under UV light. To prevent interference from inorganic carbon, the sample is acidified with 6 M phosphoric acid to reach a pH of 2 prior removing the inorganic

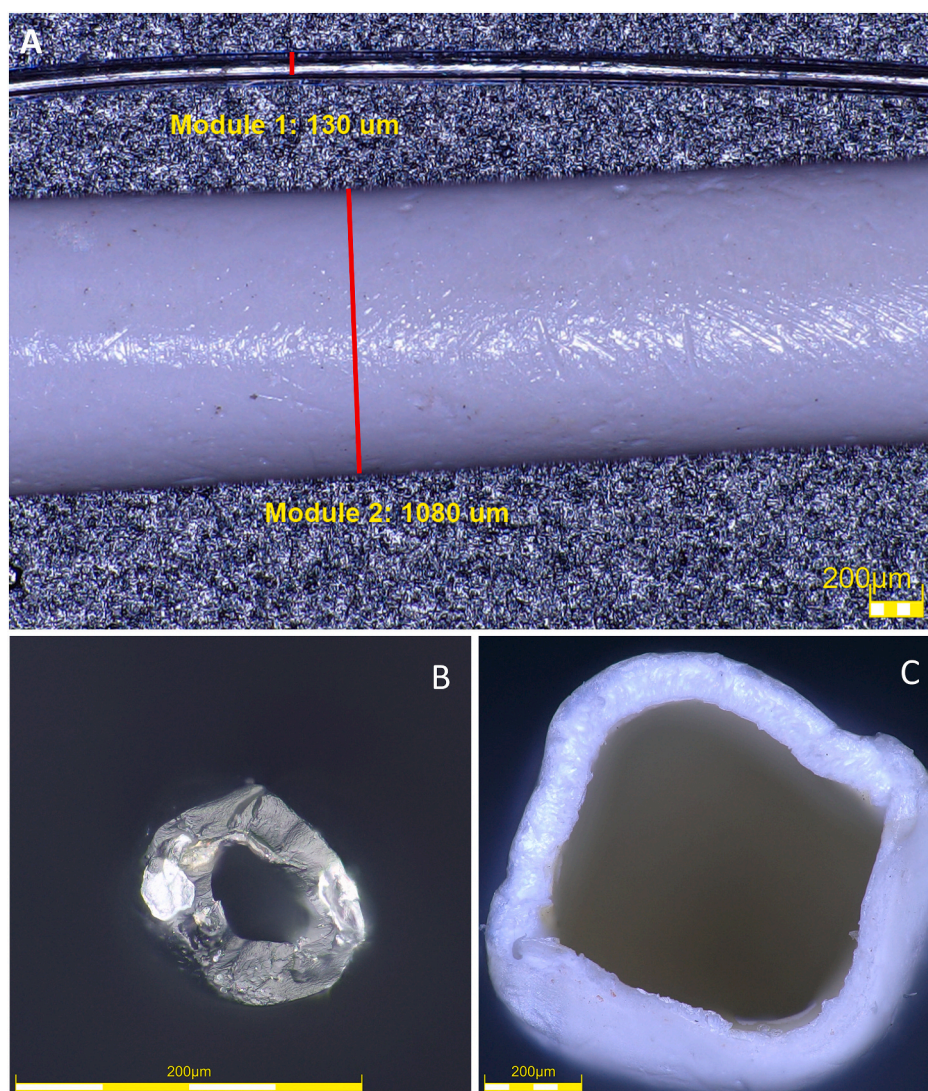


Fig. 3. Microscope images of the fibers. A) Comparison between Module 1 and Module 2 fibers. B) Module 1 – cross section, C) Module 2 – cross section.

Table 3
Summary of laboratory equipment.

Measurement	Instrument model
Inorganics	
pH and conductivity	Orion 3-star meter, Thermo Scientific
Turbidity	Turbidimeter, Thermo Scientific
Dissolved ions (chloride, sodium, sulfate, phosphate, calcium, magnesium)	Ion chromatography, ICS 6000, Thermo Scientific
Metals (iron, strontium)	Inductively coupled plasma (ICP), iCap 6500 Duo, Thermo Scientific
Residual chlorine	DR 900 - method 8021, Hach
Organics	
Total organic carbon/nitrogen	TOC-V, Shimadzu
Liquid chromatography – organic carbon detector (LC-OCD)	Suez M9 SEC, Toyo-Pearl column resin

carbon via vacuum degasser.

After the removal of inorganic carbon, ammonium persulfate is added to the acidified sample before entering a quartz reactor where organics are oxidized in the presence of UV light (185 and 254 nm). Once all the organics are oxidized to CO₂, the sample flows through a selective CO₂ permeable membrane; the CO₂ passes through the membrane where it is measured via a conductivity sensor and from that

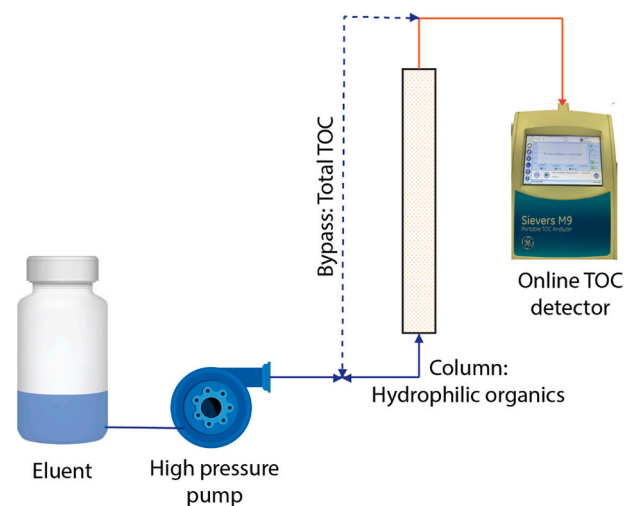


Fig. 4. Liquid chromatography with organic carbon detection (LC-OCD).

measurement, the total organic carbon is calculated. To avoid accumulation of CO₂ in the measuring loop, the solution flows through an ion exchange resin, keeping the measuring loop ion free.

For the determination of the total organic carbon (TOC), the sample is injected into the system bypassing the separation column. For the determination of the different hydrophilic organic compounds, the sample is sent through the separation column generating a chromatograph for the hydrophilic organics. The hydrophobic organics, define as those organics that do not elute from the column during the 200 min runtime, are determined by subtracting the concentration of the hydrophilic organics from the total TOC. The schematic of the system is shown in Fig. 4.

3. Theoretical model

A model, developed and verified in a previous study [46] (available for download at Mendeley Data: <https://doi.org/10.17632/f4w9mr5z3t> [47]), was applied to validate the pilot test results related to membrane permeability, fouling and cleanability. This model facilitated the comparison of the two pilot FO modules since it allows the normalization of the membrane flux and RSF based on the theoretical expected values, by accounting for the variability of the FS and DS as well as temperature fluctuations.

The membrane performance for each test was compared to the predicted value from the model since the experiments were conducted at different temperatures, due to seasonal variations (18 °C to 30 °C), and that translated to slightly different fluxes.

The developed model was designed to predict flux, feed and draw solutions effluent flows, and concentrations as well as the projected FS recovery and DS dilution at varying operating conditions (e.g., temperature and initial DS and FS salinities). Since the model can predict membrane performance (i.e., flux) at varying conditions, such capability was utilized to verify whether the change in flux during the actual WW test was solely due to membrane fouling. Similarly, it was also applied to check if the membrane's lost flux was restored after chemical cleaning.

In the model, water flux (J_w) is calculated based on Eq. 1, for cases when the active layer faces the feed solution (ALFS) or eq. 2 for cases when the active layer faces the draw solution (ALDS) [53].

$$J_w = K_m \ln \left(\frac{A \Pi_{draw} + B}{A \Pi_{feed} + J_w + B} \right) \quad (\text{ALFS}) \quad (1)$$

$$J_w = K_m \ln \left(\frac{A \Pi_{draw} - J_w + B}{A \Pi_{feed} + B} \right) \quad (\text{ALDS}) \quad (2)$$

where K_m is the mass transfer coefficient, A is the membrane water permeability, B is the salt permeability, and Π_{feed} and Π_{draw} are the osmotic pressures for the feed and draw solutions respectively. The model also considered the effect of temperature on performance by entering A and B as a function of temperature; the model assumes the same temperature for both feed and draw solutions.

For salt passage through the membrane, Eq. 3 is used to calculate the solute flux (J_s) [53].

$$J_s = \frac{B}{A \beta R T} J_w \quad (3)$$

where β is the van't Hoff coefficient, T is the absolute temperature and R is the universal gas constant.

Due to the large membrane area of the commercial modules, the feed and draw solution concentrations changes as the water flow through the module. To take that into consideration, the model divides the membrane in small discrete sections (Δm) and applied the equations for each section, providing a flux and concentration profile across the module (Fig. 5).

The model can predict performance in two different flow configurations: co-current and counter-current. For co-current flow, the water and solute flux are calculated for each discrete section (Δm) using Eq. 1, 2 and 3, and then the flows and concentrations leaving each section are calculated through Eq. 4, 5, 6 and 7 (Fig. 5).

$$FF_{i+1} = FF_i - J_w \Delta m \quad (4)$$

$$DF_{i+1} = DF_i + J_w \Delta m \quad (5)$$

$$FC_{i+1} = \frac{FC_i FF_i + J_s \Delta m}{FF_{i+1}} \quad (6)$$

$$DC_{i+1} = \frac{DC_i DF_i - J_s \Delta m}{DF_{i+1}} \quad (7)$$

where FF and DF are the flows for the feed and draw solutions respectively and FC and DC are the concentrations of NaCl for the feed and draw solutions for each section respectively.

The determination of the key model outputs in counter-current mode

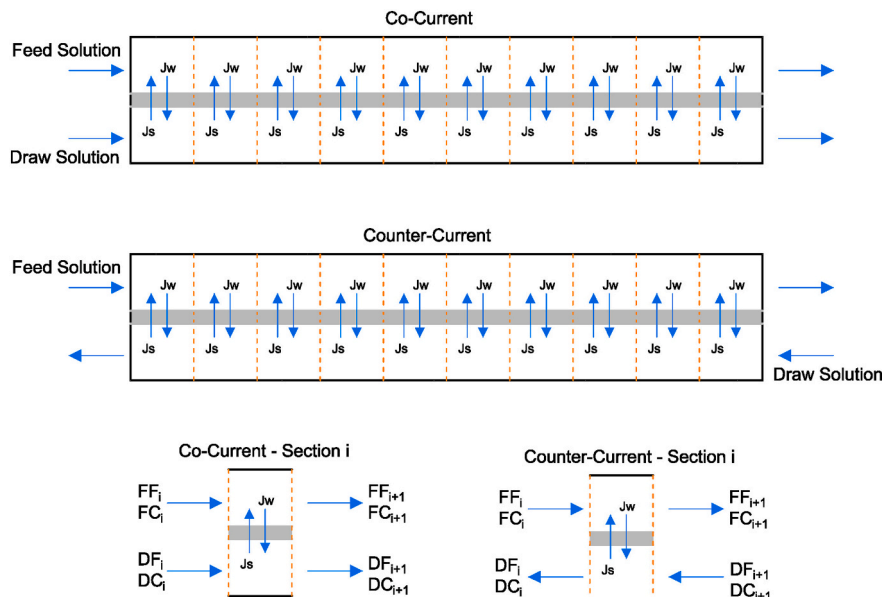


Fig. 5. Membrane sections for co-current and counter-current configurations [46].

is achieved through an iterative process. The inlet flowrates and concentrations for the feed and draw solutions are used as initial points and the model estimate the initial output values assuming co-current operation mode. The water and solute fluxes are calculated for each discrete section (Δm) using eqs. 1, 2 and 3; and to calculate the flowrates and concentrations, eqs. 4, 6, 8 and 9 are used. The output values of the model are compared with the input flowrates and concentrations of the draw solutions; if they are not within the tolerance limits (1 mg/L for the concentration and 0.1 mL/min for the flow rate), then root finding methods are used to estimate the draw solution outlets and the process iterates until the draw solution concentrations are within the tolerance limits. A process flowchart for the model has been reported in our previous publication [46].

$$DF_{i+1} = DF_i - J_{wi} \Delta m \quad (8)$$

$$DC_{i+1} = \frac{DC_i DF_i + J_{si} \Delta m}{DF_{i+1}} \quad (9)$$

The osmotic pressure for both feed and draw solutions are calculated using Eq. 10 [54]:

$$\Pi = -\phi \frac{RT}{V_w} \ln(X_w) \quad (10)$$

where Π is the osmotic pressure, ϕ is the osmotic coefficient, V_w is the volume of water per mole (also known as partial molar volume), X_w is the mole fraction of water. To account for the changes of temperature and concentrations, the osmotic coefficient (ϕ) and water density (needed for the partial molar volume determination) are obtained from the data generated by Pitzer et al. [55] by interpolating between the closest points. Those calculations assumes that the feed and draw solution contains only NaCl. The Stokes-Einstein Eq. [56] is used to calculate the diffusivities of NaCl according to Eq. 11:

$$D = \frac{K_B T}{6\pi\eta r} \quad (11)$$

where D is the diffusivity of NaCl, K_B is the Boltzmann's constant, r is the stokes radius (0.16 nm for NaCl [57]), and η is the dynamic viscosity, determined using the correlation developed by Ozbeck et al. [58].

Before being able to predict module performance, the mass transfer coefficient (K_m) and structural parameter (S) need to be fitted with a known flux value and the A and B parameters (as function of temperature). The fitting of the model is also performed via an iteration process to ensure accuracy of the predictions and to account for the hydrodynamic conditions of the module. The correlation between the mass transfer coefficient (K_m) and structural parameter (S) is shown in Eq. 12 [30].

$$K_m = \frac{D}{S} \quad (12)$$

4. Results & discussion

4.1. Benchmark performance – Synthetic solutions

The membranes' integrity and stability were evaluated through benchmark performance tests prior to actual WW testing. Long-term tests (50 h of continuous operation) were conducted using synthetic feed and draw solutions targeting 75% FS recovery. In some cases, the synthetic feed and draw solutions were slightly higher or lower than the target due to small variability in the preparation volume (5 m³) in the field. However, those changes in the concentrations were within 5% and were accounted for during the normalization through the model. Fig. 6 compares the experimental benchmark flux against the model-predicted flux for both Modules. The figure also presents the variation in salinity of feed and draw solutions during the test. For Module 1 the flux started at 1.8 L/m²·h and decreased slightly due to the dilution of DS as verified by

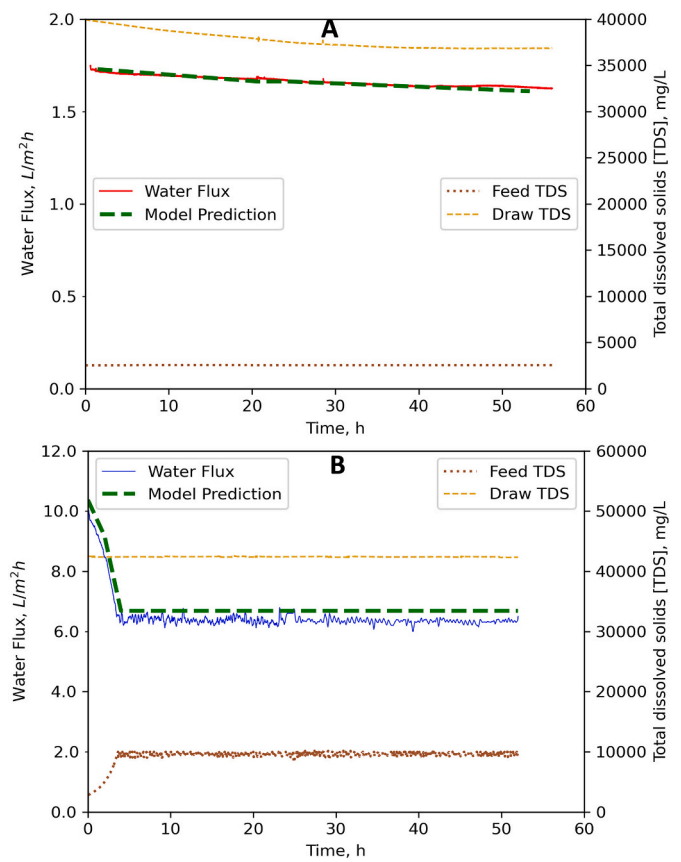


Fig. 6. Model and pilot-scale test results for: A) Module 1 and B) Module 2, using benchmark conditions (Synthetic FS: 2000 mg/L NaCl and DS: 40,000 mg/L NaCl).

the performance model (Fig. 6A). The average water flux for Module 1 was measured at 1.7 L/m²·h. Module 2 showed ~4× higher benchmark flux at 6.4 L/m²·h (Fig. 6B). Since Module 2 has the feed solution in feed and bleed mode, the first 3 h of the test are considered the concentration phase before reaching steady state performance. Due to their chemical properties, TFC membranes have higher water flux compared to CTA [59]. These findings agree with earlier studies confirming the higher permeability of TFC-based membranes against CTA [45,60]. Data for both modules showed good agreement with model predictions which confirms the model's accuracy.

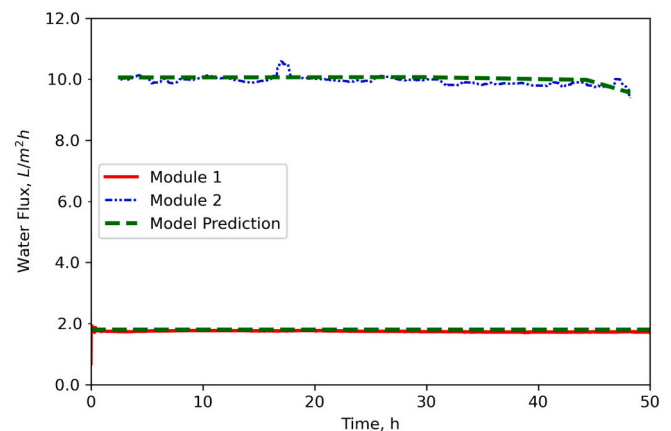


Fig. 7. Model and pilot-scale test results for Module 1 and 2 using Industrial WW (Actual FS: 946 mg/L and synthetic DS: 40,000 mg/L NaCl).

4.2. Pilot-testing performance - actual WW

Following the benchmark test, both modules were evaluated on actual industrial WW targeting the same FS recovery of 75%. Fig. 7 presents the pilot testing results for both membranes compared to the model. Average stable fluxes of 1.7 and 9.9 L/m²·h were obtained for CTA (Module 1) and TFC (Module 2) chemistries, respectively, during a 50-h test. For Module 2, the higher flux obtained with the real WW in comparison to the benchmark is attributed to the lower salinity of the actual WW (TDS: 946 vs 2000 mg/L - Table 1) that enhances the driving force across the membrane. Since module 1 operates in one-pass configuration the impact of the feed solution recovery on the water flux is not as significant as in module 2, which operates in feed and bleed mode. For module 2, the membrane is constantly exposed to the concentrated brine (at the target recovery), while in module 1, the feed concentration is changing as the water flows through the module and only the final section is exposed to the TDS concentration at the target recovery.

Experimental data were also correlated with the performance model prediction and found to be comparable (i.e., <5% deviation). Since the performance model assumes that all the TDS in the solutions is NaCl, some minor deviations on the water flux and RSF (for the industrial wastewater) are expected due to other ions present in the industrial wastewater. The predictions are expected to be more accurate for the benchmark tests since those solutions only contain NaCl.

4.3. Membrane fouling and chemical cleaning efficiency

A second benchmark test was conducted in order to assess the fouling propensity of the actual WW on the tested membranes. Tests were

performed following similar operating conditions as the initial benchmark using synthetic feed and draw solutions. Fig. 8A and Fig. 8B present the final benchmark flux results for Module 1 and 2, respectively. Experimental data were also validated with model predictions and compared based on flux loss. In Fig. 8A, the final benchmark flux for Module 1 was at 1.6 L/m²·h with ~13% flux loss from the model predicted flux at 1.8 L/m²·h which indicates fouling of Module 1. On the contrary, in Fig. 8B the final benchmark for Module 2 was at 7.4 L/m²·h, less than 5% flux loss from the model prediction at 7.6 L/m²·h. This indicates that Module 2 was apparently less susceptible to fouling in comparison to Module 1 possible due to different membrane chemistries and enhanced module hydrodynamics (since it operates at higher flow rates) which can minimize fouling.

Since the operating conditions are changing slightly (temperature and FS/DS concentrations), it is not possible to determine fouling by just comparing the absolute fluxes. The flux should be compared against the expected theoretical flux from the model which account for the process variabilities; significant deviations from the model predictions were considered fouling.

As noted earlier, both organic and inorganic membrane chemical cleaning procedures were followed to recover lost flux. Upon applying SDS surfactant cleaning on the Module 1, no improvement on membrane flux was observed and similar flux loss (~13%) compared to the model was still present. With the application of citric acid cleaning, the membrane flux was recovered back to 1.8 L/m²·h, matching the model prediction. This observation indicates that the type of fouling occurred on the Module 1 was mainly inorganics in nature. Similarly, Module 2 showed minimum fouling behavior (<5%) and citric acid cleaning showed no significant improvement on the water flux.

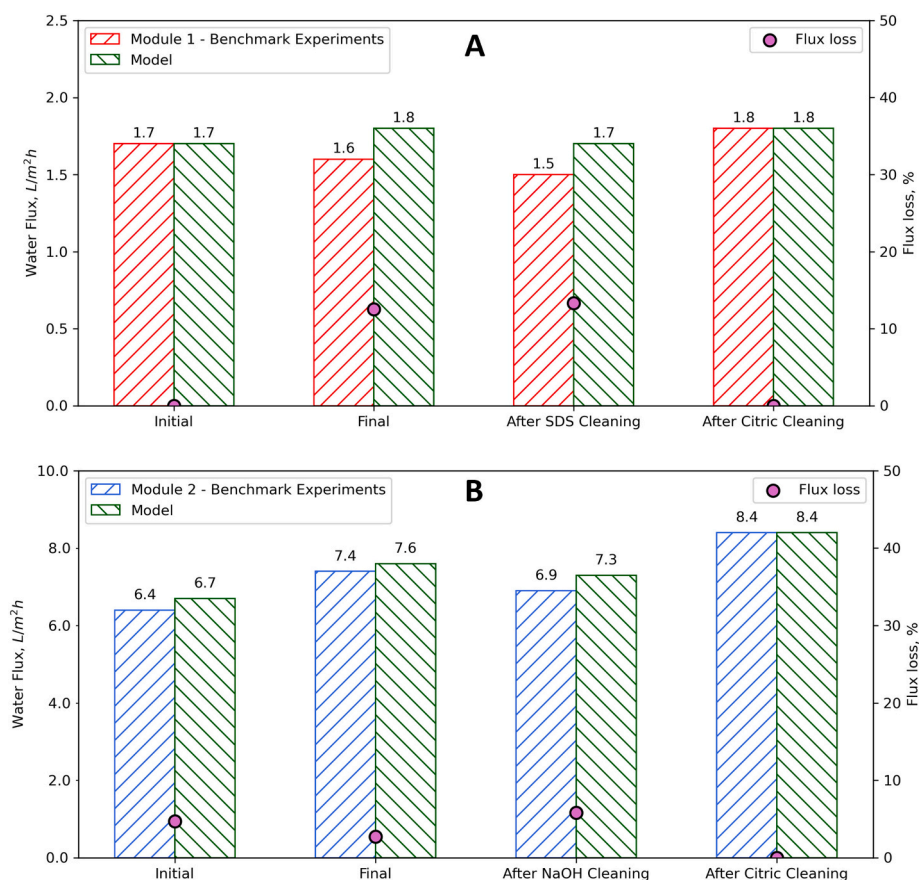


Fig. 8. Model and pilot-scale test results for initial benchmark, final benchmark, and chemical cleaning (NaOH/SDS followed by citric acid) for A) Module 1 and B) Module 2 (Synthetic FS: 2000 mg/L and synthetic DS: 40,000 mg/L NaCl).

4.4. Inorganic analysis

To confirm the possibility of inorganic fouling, the water quality was modeled using OLI, an electrolyte simulation software, to determine the scaling potential of the industrial wastewater. Before concentration, the scale potential was below the thermodynamic limit; however, after reaching 75% recovery, OLI predicts potential scaling of calcium phosphate salts; with a scale tendency $36,000\times$ higher than the thermodynamic limit; and if we considered external concentration polarization, the scaling tendency could be higher [61]. Calcium phosphate could precipitate in many forms, Hydroxyapatite, $\text{Ca}_{10}(\text{PO}_4)_6(\text{OH})_2$, is the most common one [62]; however researchers have reported that the amorphous form, CaPO_4 , could also precipitate in the membrane surface [63]. The kinetics of calcium phosphate depend on various parameters including pH, temperature, calcium and phosphate concentrations, among others [64]. Researchers have reported calcium rate loss as low as $0.35 \mu\text{mol}/\text{min}$ ($14 \mu\text{g}/\text{min}$) when seeding crystals are not present, but the rate increases significantly once the first crystals are formed [65]. The slow precipitation kinetics of calcium phosphate could translate to slow decline in flux over time.

Table 4 showed the RSF for feed solution. Positive values indicate ion flowing from the DS to FS while negative values referred to ions flowing from the FS to the DS. The ions with the highest reverse solute fluxes were sodium and chloride since those are the primary ions in the synthetic DS. For Module 1, the negative RSF for calcium and phosphate is attributed to calcium phosphate precipitation, which was responsible for the flux loss after the actual WW test.

As seen in Table 4, Module 2 has lower RSF for most (majority) of inorganics as compared to Module 1; in agreement with the higher rejection capabilities of the TFC membranes [29]. Also, Module 2 has a higher rejection of sulfate ions; Module 2 has a sulfate specific forward flux of $56 \text{ mg}/\text{L}$ vs $90 \text{ mg}/\text{L}$ from Module 1.

4.5. Organic characterization analysis

To assess the impact of organics on membrane performance, the feed solution before and after the treatment was analyzed using an advanced organic characterization technique, LC-OCD, to classify the organics based on their hydrophobicity and hydrophilicity. Results showed that the feed water contains a total organic carbon content of $8.1 \text{ mg}/\text{L}$ and from those, $7.9 \text{ mg}/\text{L}$ are hydrophilic (organics that prefer the water phase based on the interaction with the separation column) [66], and only $0.2 \text{ mg}/\text{L}$ are considered hydrophobic. The hydrophobic organics are typically more problematic for membranes since they tend to adhere on the membrane surface [66]. Due to the low concentration of hydrophobic organics, organic fouling was not expected.

The hydrophilic organics can be further characterized based on their

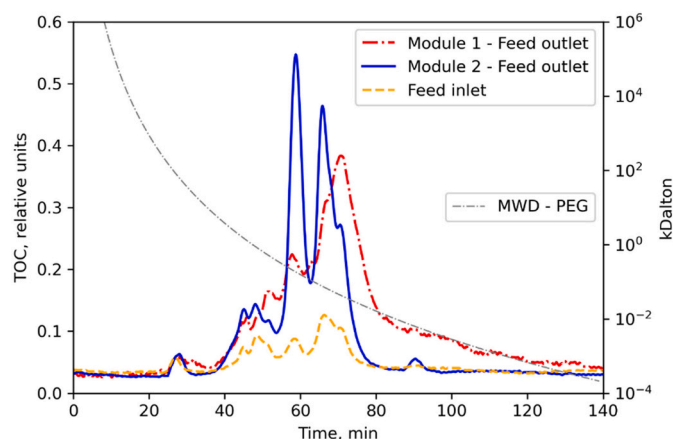


Fig. 9. Organic Characterization data for inlet feed and concentrated feed, including expected molecular weight distribution (MWD) based on Polyethylene Glycol (PEG).

molecular weights by size exclusion chromatography. Fig. 9, showing the chromatograph of the hydrophilic organics, reveals that the concentrated feed of the Module 2 has a similar distribution as the initial feed solution; the increase on each peak area is approximately $4\times$ which correspond to the concentration factor of the industrial wastewater (75% recovery). For Module 2, the only peak that did not increase was the peak at 28 min, equivalent to polyethylene glycol (PEG) molecular weight (MW) of approximately 62 kDa, which could be attributed to organics passing through the membrane. Based on mass balance calculations (Table 4), Module 2 shows an organic specific forward flux of $0.1 \text{ mg}/\text{L}$ which could be attributed to the portion of the hydrophilic organics not matching the expected 75% recovery.

On the other hand, the chromatograph for the concentrated feed of the Module 1 does not show a $4\times$ increase on the peak areas for most of the peaks. The peak eluting at 60 min, equivalent to a PEG MW of 150 Da, is approximately $2\times$ larger than the feed one (instead of the expected $4\times$), which could be due to organics passing through the membrane. Similar observation can be drawn for peaks eluting before 60 min, which may be only partially rejected by the membranes. The peak at approximately 70 min, equivalent to PEG MW of 50 Da, has an area of around $4\times$ that of the feed highlighting that it may have been rejected by the membrane. Since the cleaning procedure for organic removal did not show an increase in membrane performance, those organics may not be deposited on the membrane.

Compared to Module 2, Module 1 has a specific organic forward flux of $0.9 \text{ mg}/\text{L}$, which is significantly higher compared to $0.1 \text{ mg}/\text{L}$ from Module 1 (Table 4). That is consistent with the higher rejection capabilities of TFC membranes compared to CTA [67].

4.6. Considerations for full-scale implementation

OC process is capable of successfully reducing wastewater disposal volumes from oil & gas operations. However, for full-scale implementation, certain factors should be considered for a successful cost-effective deployment of the technology to reduce the volume of industrial wastewater (Fig. 10) as compared to RO. Those factors include:

4.6.1. Low energy

Energy is one of the key factors governing the economics of OC. Since OC runs at ambient pressure, the energy needed is significantly lower compared to RO. Based on the pump energy requirements [26,68], OC operating at 1 bar pressure, requires 6.3 kWh for a $2000 \text{ m}^3/\text{day}$ processing plant. For the same capacity, a low-pressure RO plant, operating at 15 bars, requires 46 kWh .

The lower energy demand helps in reducing the operating cost

Table 4

Membrane reverse solute flux (RSF) on industrial wastewater.

Positive values: ions flowing from the DS to FS. Negative values: ions flowing from the FS to the DS.

Parameter	Module 1		Module 2	
	RSF	Specific RSF	RSF	Specific RSF
	$\text{mmol}/(\text{m}^2 \cdot \text{h})$	mg/L	$\text{mmol}/(\text{m}^2 \cdot \text{h})$	mg/L
Na^+	5.7	75	37	78
Ca^{2+}	-0.01	-0.2	0.3	1.1
Mg^{2+}	-0.08	-1.1	-0.2	-0.3
Cl^-	7.6	156	25	81
SO_4^{2-}	-1.6	-90	-6.4	-56
PO_4^{3-}	-0.01	-0.8	0	0
Total organic carbon	-0.2	-0.9	-0.1	-0.1

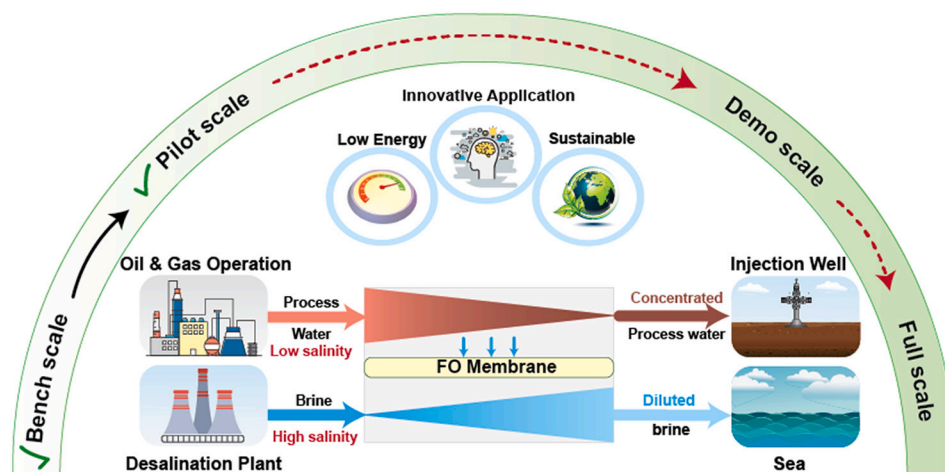


Fig. 10. Diagram showing the current state of osmotic concentration for the treatment of industrial wastewater including the considerations for full scale implementation.

[69–71]; an MBR-FO system could have a net present value (NPV) 20% lower than MBR-RO [70].

4.6.2. Sustainability

OC can be a sustainable process since it is capable of minimizing greenhouse gas (GHG) emissions associated with water volume reduction by decreasing energy required for the treatment compared to the state-of-the-art RO [72]. Assuming that the electricity is generated by a clean burning fuel, natural gas (400 gCO₂/KWh) [73], that would translate to 30 gCO₂/m³. This emission is 7× lower compared to low pressure RO, operating at 15 bar, which has an emission of 222 gCO₂/m³.

Another sustainable aspect of the process is the beneficial dilution of the brine discharged to the Arabian Gulf. The process is capable of diluting the brine up to 75%, depending on the feed and draw solution concentrations [46,49,74]. This environmental benefit minimizes the impact on the marine life and enable alternative disposal options, making OC an attractive process for future project developments.

4.6.3. Innovative application

OC has its niche application in places where the low salinity produced, or process water are available. Those water sources could be ideal for a volume reduction process due to the low salt content [23].

Another key aspect is to have the low salinity stream near a draw solution (i.e., seawater or desalination brine). In Qatar, the gas production facilities are nearby to full-scale water desalination plants, which makes it feasible to implement the OC process at full-scale.

For the wastewater evaluated, OC could reduce its volume up to 75%, enhancing the life of the disposal wells beyond current advanced treatment process (MBR-RO) that targets 60% volume reduction. To advance the TRL of OC for this application, a demonstration-scale testing in the field, under relevant conditions, is currently being planned to obtain a detailed economic assessment and validate the performance parameters of the technology.

5. Conclusions

This study presented a side-by-side performance evaluation of two commercial HF - FO membranes at pilot scale for actual wastewater volume reduction from oil & gas operations. A theoretical model was used to normalize and compare the performance data of the two modules taking into consideration the variability of the operating conditions. The key outcomes of the project were:

- Long-term benchmark tests (50 h of continuous operation), conducted using synthetic feed and draw solutions, showed good agreement between the experimental data and model prediction. Less than 5% deviation between the theoretical and experimental values were observed.
- Performance tests conducted using actual wastewater from a gas production facility showed that Module 2 (TFC) has a higher flux compared to Module 1 (CTA), 9.9 L/m²·h vs 1.7 L/m²·h; and lower specific RSF for most of the ions.
- Module 1 benchmark test (after the actual WW) showed a 13% flux loss compared to the model predicted value, the flux loss was attributed to inorganic membrane fouling (calcium phosphate precipitation). The loss of flux for Module 2 was <5% possible due to difference in membrane chemistry and to enhanced hydrodynamics within the module (since it operates at higher flow rates).
- For Module 1, chemical cleaning (citric acid) proved to be successful in restoring the flux back to their initial performance.
- From the 8.1 mg/L organic carbon present in the feed, organic characterization analysis reveals that certain group of hydrophilic organics are able to pass through Module 1, but not Module 2, translated to a specific forward organic solute flux of 0.9 mg/L and 0.1 mg/L for Module 1 and 2, respectively.

For volume reduction of industrial WW, OC has lower energy consumption compared to RO since it operates at ambient pressure. OC is also a more sustainable process since it reduces the greenhouse gas emissions, and it is able to dilute the brine discharged. OC has its niche application in places where the low salinity industrial WW are in close proximity to a high salinity brine to serve as draw solution. Finally, the OC process has strong potential for full-scale installation; however, demonstrating the technology in the field would be the next step for successful implementation of the technology.

Nomenclature

A	water permeability coefficient [L/(m ² h bar)]
B	salt permeability coefficient [L/(m ² h)]
D	diffusion constant [m ² /s]
DC	draw concentration [mol/L]
DF	draw flowrate [L/min]
FC	feed concentration [mol/L]
FF	feed flowrate [L/min]
i	discrete section number
J _s	solute flux [mol/(m ² h)]

J_w	water flux [L/(m ² h)]
K_B	Boltzmann's constant [(m ² kg)/(K s ²)]
K_m	mass transfer coefficient [L/(m ² h)]
r	Stokes radius [m]
R	universal gas constant [(L bar)/(K mol)]
S	structural parameter [m]
T	temperature [K]
V_w	volume of water per mole (partial molar volume) [L/mol]
X_w	mole fraction of water
β	van't Hoff coefficient
Δm	discrete membrane area [m ²]
η	dynamic viscosity [kg/(m s)]
Π	osmotic pressure (bar)
ϕ	osmotic coefficient

CRedit authorship contribution statement

Joel Minier-Matar: Writing – original draft, Methodology, Investigation, Software, Formal analysis, Visualization. **Masha'al Al-Maas:** Writing – original draft, Investigation, Software, Formal analysis, Visualization. **Altaf Hussain:** Writing – original draft, Resources. **Mustafa S. Nasser:** Project administration, Funding acquisition. **Samer Adham:** Conceptualization, Methodology, Supervision, Project administration, Funding acquisition, Writing – review & editing.

Declaration of competing interest

The authors declare that they have no known competing financial interests or personal relationships that could have appeared to influence the work reported in this paper.

Acknowledgments

This work was made possible by National Priorities Research Program (NPRP) grant NPRP 10-0118-170191 from the Qatar National Research Fund (a member of Qatar Foundation). The findings achieved herein are solely the responsibility of the authors and do not necessarily represent the official views of ConocoPhillips or the Qatar National Research Fund.

The research team would like to acknowledge their colleagues at the ConocoPhillips Global Water Sustainability Centre including: Arnie Janson, Nabin Upadhyay, Eman AlShamari for their support with the testing and lab analyses.

The authors would like to thank Abdelrahman Awad, Reem Jalab and Dan Cortes from Qatar University for their support with the pilot evaluation.

The project team would like to thank Simon Judd, at Judd & Judd Limited, for his contributions to the project. Also, thanks to Toyobo and Aromatec teams for the technical support provided during the evaluation. Open Access funding provided by the Qatar National Library.

References

- [1] J.A. Veil, M.G. Puder, D. Elcock, R.J. Redweik Jr., A White Paper Describing Produced Water from Production of Crude Oil, Natural Gas, and Coal Bed Methane, Argonne National Lab, IL (US), 2004.
- [2] R. Ahmadizadeh, S. Shokrollahzadeh, S.M. Latifi, Forward osmosis performance in extracting water from produced water, *J. Appl. Water Eng. Res.* (2021) 1–9.
- [3] S. Adham, A. Hussain, J. Minier-Matar, A. Janson, R. Sharma, Membrane applications and opportunities for water management in the oil & gas industry, *Desalination*. (2018), <https://doi.org/10.1016/j.desal.2018.01.030>.
- [4] R. Does, A. Hussain, M. Katebah, S.S. Adham, Using advanced water treatment technologies to treat produced water from the petroleum industry, *SPE Int. Prod. Oper. Conf. Exhib.* (2012), <https://doi.org/10.2118/157108-MS>.
- [5] A. Hussain, J. Minier-Matar, A. Janson, S. Adham, Treatment of produced water from oil & gas operations by membrane distillation, *Proc. 4th Int. Gas Process. Symp.* (2015), <https://doi.org/10.1016/b978-0-444-63461-0.50029-8>.
- [6] A. Hussain, J. Minier-Matar, S. Gharfeh, A. Janson, S. Adham, Advanced technologies for produced water treatment, in: *Offshore Technol. Conf.*, 2014, <https://doi.org/10.4043/24749-ms>.
- [7] W.C. Lyons, G.J. Plisga, *Standard Handbook of Petroleum and Natural Gas Engineering*, Elsevier, 2011.
- [8] C.J.A. Furtado, A. Siqueira, A.L.S. de Souza, A.C. Correa, R. Mendes, Produced water reinjection in petrobras fields: challenges and perspectives, in: *SPE Lat. Am. Caribb. Pet. Eng. Conf., OnePetro*, 2005.
- [9] R.E. Mace, J.-P. Nicot, A.H. Chowdhury, A.R. Dutton, S. Kalaswad, Please Pass the Salt: Using Oil Fields for the Disposal of Concentrate from Desalination Plants. <https://www.usbr.gov/research/dwpr/reportpdfs/report112.pdf>, 2005.
- [10] J.M. Sheikhan, I. Zainab, A. Janson, S. Adham, et al., Qatargas wastewater treatment plants: an advanced design for water reuse, in: *Int. Pet. Technol. Conf.*, 2015.
- [11] L.D. Nghiem, T. Ren, N. Aziz, I. Porter, G. Regmi, Treatment of coal seam gas produced water for beneficial use in Australia: a review of best practices, *Desalin. Water Treat.* 32 (2011) 316–323.
- [12] M. Wenzlick, N. Siefert, Techno-economic analysis of converting oil & gas produced water into valuable resources, *Desalination*. 481 (2020), 114381, <https://doi.org/10.1016/j.desal.2020.114381>.
- [13] J. Shi, W. Huang, H. Han, C. Xu, Review on treatment technology of salt wastewater in coal chemical industry of China, *Desalination*. 493 (2020), 114640, <https://doi.org/10.1016/j.desal.2020.114640>.
- [14] G. Pérez, P. Gómez, I. Ortiz, A. Uriaga, Techno-economic assessment of a membrane-based wastewater reclamation process, *Desalination*. 522 (2022), 115409, <https://doi.org/10.1016/j.desal.2021.115409>.
- [15] X. Wei, K.T. Sanders, A.E. Childress, Reclaiming wastewater with increasing salinity for potable water reuse: water recovery and energy consumption during reverse osmosis desalination, *Desalination*. 520 (2021), 115316, <https://doi.org/10.1016/j.desal.2021.115316>.
- [16] H.S. Son, M.W. Shahzad, N. Ghaffour, K.C. Ng, Pilot studies on synergetic impacts of energy utilization in hybrid desalination system: multi-effect distillation and adsorption cycle (MED-AD), *Desalination*. 477 (2020), 114266, <https://doi.org/10.1016/j.desal.2019.114266>.
- [17] J. DeCarolis, S. Adham, W.R. Pearce, Z. Hirani, S. Lacy, R. Stephenson, Cost trends of MBR systems for municipal wastewater treatment, *Proc. Water Environ. Fed.* 15 (2007) 3407–3418.
- [18] B. Alspach, S. Adham, T. Cooke, P. Delphos, J. Garcia-Aleman, J. Jacangelo, A. Karimi, J. Pressman, J. Schaefer, S. Sethi, Microfiltration and ultrafiltration membranes for drinking water, *J. Am. Water Works Assoc.* 100 (2008) 84–97.
- [19] H. Nassrullah, S.F. Anis, R. Hashaikheh, N. Hilal, Energy for desalination: a state-of-the-art review, *Desalination*. 491 (2020), 114569, <https://doi.org/10.1016/j.desal.2020.114569>.
- [20] W. Suwailah, N. Pathak, H. Shon, N. Hilal, Forward osmosis membranes and processes: a comprehensive review of research trends and future outlook, *Desalination*. 485 (2020), 114455, <https://doi.org/10.1016/j.desal.2020.114455>.
- [21] L. Francis, O. Ogunbiyi, J. Saththasivam, J. Lawler, Z. Liu, A comprehensive review of forward osmosis and niche applications, *Environ. Sci. Water Res. Technol.* 6 (8) (2020) 1986–2015.
- [22] J.E. Kim, S. Phuntsho, L. Chekli, S. Hong, N. Ghaffour, T.O. Leiknes, J.Y. Choi, H. K. Shon, Environmental and economic impacts of fertilizer drawn forward osmosis and nanofiltration hybrid system, *Desalination*. 416 (2017) 76–85, <https://doi.org/10.1016/j.desal.2017.05.001>.
- [23] D.L. Shaffer, J.R. Werber, H. Jaramillo, S. Lin, M. Elimelech, Forward osmosis: where are we now? *Desalination*. 356 (2015) 271–284, <https://doi.org/10.1016/j.desal.2014.10.031>.
- [24] A. Mahto, K. Aruchamy, R. Meena, M. Kamali, S.K. Nataraj, T.M. Aminabhavi, Forward osmosis for industrial effluents treatment – sustainability considerations, *Proc. Purif. Technol.* 254 (2021), 117568, <https://doi.org/10.1016/j.seppur.2020.117568>.
- [25] F. Lotfi, L. Chekli, S. Phuntsho, S. Hong, J.Y. Choi, H.K. Shon, Understanding the possible underlying mechanisms for low fouling tendency of the forward osmosis and pressure assisted osmosis processes, *Desalination*. 421 (2017) 89–98, <https://doi.org/10.1016/j.desal.2017.01.037>.
- [26] J. Minier-Matar, A. Santos, A. Hussain, A. Janson, R. Wang, A.G. Fane, S. Adham, Application of hollow fiber forward osmosis membranes for produced and process water volume reduction: an osmotic concentration process, *Environ. Sci. Technol.* 50 (2016), <https://doi.org/10.1021/acs.est.5b04801>.
- [27] S. Zhao, J. Minier-Matar, S. Chou, R. Wang, A.G. Fane, S. Adham, Gas field produced/process water treatment using forward osmosis hollow fiber membrane: membrane fouling and chemical cleaning, *Desalination*. 402 (2017) 143–151, <https://doi.org/10.1016/j.desal.2016.10.006>.
- [28] J. Minier-Matar, A. Hussain, A. Janson, R. Wang, A.G. Fane, S. Adham, Application of forward osmosis for reducing volume of produced/process water from oil and gas operations, *Desalination*. 376 (2015), <https://doi.org/10.1016/j.desal.2015.08.008>.
- [29] B.D. Coday, P. Xu, E.G. Beaudry, J. Herron, K. Lampi, N.T. Hancock, T.Y. Cath, The sweet spot of forward osmosis: treatment of produced water, drilling wastewater, and other complex and difficult liquid streams, *Desalination*. 333 (2014) 23–35, <https://doi.org/10.1016/j.desal.2013.11.014>.
- [30] R. Wang, L. Shi, C.Y. Tang, S. Chou, C. Qiu, A.G. Fane, Characterization of novel forward osmosis hollow fiber membranes, *J. Membr. Sci.* 355 (2010) 158–167, <https://doi.org/10.1016/j.memsci.2010.03.017>.
- [31] F. Lotfi, S. Phuntsho, T. Majeed, K. Kim, D.S. Han, A. Abdel-Wahab, H.K. Shon, Thin film composite hollow fibre forward osmosis membrane module for the desalination of brackish groundwater for fertigation, *Desalination*. 364 (2015) 108–118, <https://doi.org/10.1016/j.desal.2015.01.042>.

- [32] B.D. Coday, D.M. Heil, P. Xu, T.Y. Cath, Effects of transmembrane hydraulic pressure on performance of forward osmosis membranes, *Environ. Sci. Technol.* 47 (2013) 2386–2393, <https://doi.org/10.1021/es304519p>.
- [33] K.J. Howe, A. Marwah, K.P. Chiu, S.S. Adham, Effect of membrane configuration on bench-scale MF and UF fouling experiments, *Water Res.* 41 (2007) 3842–3849, <https://doi.org/10.1016/j.watres.2007.05.025>.
- [34] D. Dardor, M. Al Maas, J. Minier-Matar, A. Janson, A. Abdel-Wahab, H.K. Shon, S. Adham, Evaluation of pretreatment and membrane configuration for pressure-retarded osmosis application to produced water from the petroleum industry, *Desalination*. 516 (2021), 115219, <https://doi.org/10.1016/J.DESAL.2021.115219>.
- [35] A.M. Awad, R. Jalab, J. Minier-Matar, S. Adham, M.S. Nasser, S.J. Judd, The status of forward osmosis technology implementation, *Desalination*. 461 (2019) 10–21, <https://doi.org/10.1016/j.desal.2019.03.013>.
- [36] M. Zhan, Y. Kim, S. Hong, Comprehensive review of osmotic dilution/concentration using FO membranes for practical applications, *Desalination*. 515 (2021), 115190, <https://doi.org/10.1016/J.DESAL.2021.115190>.
- [37] R.L. McGinnis, N.T. Hancock, M.S. Nowosielski-Slepown, G.D. McGurgan, Pilot demonstration of the NH_3/CO_2 forward osmosis desalination process on high salinity brines, *Desalination*. 312 (2013) 67–74, <https://doi.org/10.1016/j.desal.2012.11.032>.
- [38] Oasys Water's FO technology to treat Chinese power plant's wastewater, *Pump Ind. Anal.* 2014 (2014) 3, [https://doi.org/10.1016/S1359-6128\(14\)70348-9](https://doi.org/10.1016/S1359-6128(14)70348-9).
- [39] R.A. Maltos, J. Regnery, N. Almaraz, S. Fox, M. Schutter, T.J. Cath, M. Veres, B. D. Coday, T.Y. Cath, Produced water impact on membrane integrity during extended pilot testing of forward osmosis – reverse osmosis treatment, *Desalination*. 440 (2018) 99–110, <https://doi.org/10.1016/j.desal.2018.02.029>.
- [40] M. Zhan, Y. Kim, J. Lim, S. Hong, Application of fouling index for forward osmosis hybrid system: a pilot demonstration, *J. Membr. Sci.* 617 (2021), 118624, <https://doi.org/10.1016/j.memsci.2020.118624>.
- [41] D.H. Kim, C. Lee, T.T. Nguyen, R.S. Adha, C. Kim, S.J. Ahn, H. Son, I.S. Kim, Insight into fouling potential analysis of a pilot-scale pressure-assisted forward osmosis plant for diluted seawater reverse osmosis desalination, *J. Ind. Eng. Chem.* 98 (2021) 237–246, <https://doi.org/10.1016/j.jiec.2021.03.048>.
- [42] T.P.N. Nguyen, B.M. Jun, Y.N. Kwon, The chlorination mechanism of integrally asymmetric cellulose triacetate (CTA)-based and thin film composite polyamide-based forward osmosis membrane, *J. Membr. Sci.* 523 (2017) 111–121, <https://doi.org/10.1016/J.MEMSCI.2016.09.020>.
- [43] D. Ahmed, H. Isawi, N. Badway, A. Elbayaa, H. Shawky, Highly porous cellulosic nanocomposite membranes with enhanced performance for forward osmosis desalination, *Iran. Polym. J.* 30 (2021) 423–444.
- [44] D.F. Ahmed, H. Isawi, N.A. Badway, A.A. Elbayaa, H. Shawky, Graphene oxide incorporated cellulose triacetate/cellulose acetate nanocomposite membranes for forward osmosis desalination, *Arab. J. Chem.* 14 (2021), 102995.
- [45] M. Xie, S.R. Gray, Gypsum scaling in forward osmosis: role of membrane surface chemistry, *J. Membr. Sci.* 513 (2016) 250–259, <https://doi.org/10.1016/J.MEMSCI.2016.04.022>.
- [46] J. Minier-Matar, M. Al-Maas, D. Dardor, A. Janson, M.S. Nasser, S. Adham, Industrial wastewater volume reduction through osmotic concentration: membrane module selection and process modeling, *J. Water Process Eng.* 40 (2021), 101760, <https://doi.org/10.1016/j.jwpe.2020.101760>.
- [47] J. Minier-Matar, M. Al-Maas, D. Dardor, A. Janson, M.S. Nasser, S. Adham, Forward osmosis (FO) membrane performance model, *Mendeley Data*. (2020), <https://doi.org/10.17632/f4w9mr5z3t.1>.
- [48] J.M. Sheikhan, I. Zainab, A. Janson, S. Adham, Qatargas wastewater treatment plants: an advanced design for water reuse, in: *Int. Pet. Technol. Conf.*, 2015, pp. 1–7, <https://doi.org/10.2523/iptc-18456-ms>.
- [49] R. Jalab, A.M. Awad, M.S. Nasser, J. Minier-Matar, S. Adham, Pilot-scale investigation of flowrate and temperature influence on the performance of hollow fiber forward osmosis membrane in osmotic concentration process, *J. Environ. Chem. Eng.* 8 (2020), 104494, <https://doi.org/10.1016/j.jece.2020.104494>.
- [50] D. Somwanshi, M. Bunde, G. Kumar, G. Parashar, Comparison of fuzzy-PID and PID controller for speed control of DC motor using LabVIEW, *Procedia Comput. Sci.* 152 (2019) 252–260.
- [51] J. Parodi, J.R. Mangado, O. Stefansson, M. Flynn, H. Shaw, D. Beeler, FOST 2 upgrade with hollow-fiber CTA FO module and generation of osmotic agent for microorganism growth studies, in: *46th Int. Conf. Environ. Syst.*, 2016.
- [52] S. Zhao, J. Minier-Matar, S. Chou, R. Wang, A.G. Fane, S. Adham, Gas field produced/process water treatment using forward osmosis hollow fiber membrane: membrane fouling and chemical cleaning, *Desalination*. (2017), <https://doi.org/10.1016/j.desal.2016.10.006>.
- [53] C.Y. Tang, Q. She, W.C.L. Lay, R. Wang, A.G. Fane, Coupled effects of internal concentration polarization and fouling on flux behavior of forward osmosis membranes during humic acid filtration, *J. Membr. Sci.* 354 (2010) 123–133, <https://doi.org/10.1016/j.memsci.2010.02.059>.
- [54] J. Feher, Osmosis and osmotic pressure, in: *Quant. Hum. Physiol.*, Elsevier, 2017, pp. 182–198, <https://doi.org/10.1016/B978-0-12-800883-6.00017-3>.
- [55] K.S. Pitzer, J.C. Peiper, R.H. Busey, K.S. Pitzer, J.C. Pelter, Thermodynamic properties of aqueous sodium chloride solutions thermodynamic properties of aqueous sodium chloride solutions, *J. Phys. Chem. Ref. Data* 1 (1992), <https://doi.org/10.1063/1.555709>.
- [56] C.C. Miller, The Stokes-Einstein law for diffusion in solution, in: *Proc. R. Soc. London. Ser. A, Contain. Pap. a Math. Phys. Character* 106, 1924, pp. 724–749.
- [57] Y. Marcus, Ionic radii in Aqueous solutions, *Chem. Rev.* 88 (1988) 1475–1498.
- [58] H. Ozbek, J.A. Fair, S.L. Phillips, VISCOSITY of aqueous sodium chloride solutions from 0–1500 °C, 1977.
- [59] E.A. Bell, T.E. Poynton, K.B. Newhart, J. Regnery, B.D. Coday, T.Y. Cath, Produced water treatment using forward osmosis membranes: evaluation of extended-time performance and fouling, *J. Membr. Sci.* 525 (2017) 77–88, <https://doi.org/10.1016/J.MEMSCI.2016.10.032>.
- [60] J.-Y. Li, Z.-Y. Ni, Z.-Y. Zhou, Y.-X. Hu, X.-H. Xu, L.-H. Cheng, Membrane fouling of forward osmosis in dewatering of soluble algal products: comparison of TFC and CTA membranes, *J. Membr. Sci.* 552 (2018) 213–221.
- [61] D. Wang, J. Zhang, J. Li, W. Wang, H.K. Shon, H. Huang, Y. Zhao, Z. Wang, Inorganic scaling in the treatment of shale gas wastewater by fertilizer drawn forward osmosis process, *Desalination*. 521 (2022), 115396, <https://doi.org/10.1016/J.DESAL.2021.115396>.
- [62] E.D. Eanes, in: Z. Amjad (Ed.), *Amorphous Calcium Phosphate: Thermodynamic and Kinetic Considerations* BT - Calcium Phosphates in Biological and Industrial Systems, Springer US, Boston, MA, 1998, pp. 21–39, https://doi.org/10.1007/978-1-4615-5517-9_2.
- [63] M.N. Mangal, S.G. Salinas-Rodriguez, J. Dusseldorp, A.J.B. Kemperman, J. C. Schippers, M.D. Kennedy, W.G.J. van der Meer, Effectiveness of antiscalants in preventing calcium phosphate scaling in reverse osmosis applications, *J. Membr. Sci.* 623 (2021), 119090, <https://doi.org/10.1016/J.MEMSCI.2021.119090>.
- [64] W.A. House, The prediction of phosphate coprecipitation with calcite in freshwaters, *Water Res.* 24 (1990) 1017–1023.
- [65] L.J. Plant, W.A. House, Precipitation of calcite in the presence of inorganic phosphate, *Colloids Surfaces A Physicochem. Eng. Asp.* 203 (2002) 143–153, [https://doi.org/10.1016/S0927-7757\(01\)01089-5](https://doi.org/10.1016/S0927-7757(01)01089-5).
- [66] S.A. Huber, A. Balz, M. Abert, W. Pronk, Characterisation of aquatic humic and non-humic matter with size-exclusion chromatography–organic carbon detection–organic nitrogen detection (LC-OCD-OND), *Water Res.* 45 (2011) 879–885.
- [67] M. Sauchelli, G. Pellegrino, A. D'Haese, I. Rodríguez-Roda, W. Gernjak, Transport of trace organic compounds through novel forward osmosis membranes: role of membrane properties and the draw solution, *Water Res.* 141 (2018) 65–73, <https://doi.org/10.1016/j.watres.2018.05.003>.
- [68] A. Janson, D. Dardor, M. Al Maas, J. Minier-Matar, A. Abdel-Wahab, S. Adham, Pressure-retarded osmosis for enhanced oil recovery, *Desalination*. 491 (2020), 114568, <https://doi.org/10.1016/J.DESAL.2020.114568>.
- [69] P. Pazouki, R.A. Stewart, E. Bertone, F. Helfer, N. Ghaffour, Life cycle cost of dilution desalination in off-grid locations: a study of water reuse integrated with seawater desalination technology, *Desalination*. 491 (2020), 114584, <https://doi.org/10.1016/J.DESAL.2020.114584>.
- [70] R. Jalab, A.M. Awad, M.S. Nasser, J. Minier-Matar, S. Adham, S.J. Judd, An empirical determination of the whole-life cost of FO-based open-loop wastewater reclamation technologies, *Water Res.* 163 (2019), 114879, <https://doi.org/10.1016/j.watres.2019.114879>.
- [71] S.J. Im, S. Jeong, S. Jeong, A. Jang, Techno-economic evaluation of an element-scale forward osmosis-reverse osmosis hybrid process for seawater desalination, *Desalination*. 476 (2020), 114240, <https://doi.org/10.1016/J.DESAL.2019.114240>.
- [72] N.H. Ab Hamid, S. Smart, D.K. Wang, K.W.J. Koh, K.J.C. Ng, L. Ye, Economic, energy and carbon footprint assessment of integrated forward osmosis membrane bioreactor (FOMBR) process in urban wastewater treatment, *Environ. Sci. Water Res. Technol.* 6 (2020) 153–165.
- [73] I.E. Agency, CO₂ emissions from fuel combustion highlights 2017, in: *IEA Paris, France*, 2017.
- [74] A.M. Awad, R. Jalab, M.S. Nasser, M. El-Naas, I.A. Hussein, J. Minier-Matar, S. Adham, Evaluation of cellulose triacetate hollow fiber membrane for volume reduction of real industrial effluents through an osmotic concentration process: a pilot-scale study, *Environ. Technol. Innov.* 24 (2021), 101873, <https://doi.org/10.1016/J.ETI.2021.101873>.